8 DDT Testing and Image Analysis

Introduction

This chapter looks at the output of the debris detection (DDT) program, under test conditions, and for analysis of real pictures taken at the South African Astronomical Observatory (SAAO) near Cape Town. For both test run and SAAO imagery analysis, the machine used was a Pentium PC with a clock speed of 333 MHz and 64MB of RAM, running the Linux RedHat 5.1 operating system.

8.1 Static Noise Tests

This part of the testing was purely to determine how many "false" lines the program would detect given a set of frames containing nothing but simulated noise (i.e. no debris or star tracks).

The test program was coded in C, and compiled using the GNU C compiler with the "O4" speed optimisation flag set. The program fed the DDT program a number of simulated noisy frames filled with randomly spaced dots, generated using the standard C "rand()" function. The set of frames was limited to the number of frames used to detect debris, i.e. if for example 5 frames were deemed necessary to detect debris then only 5 frames would be used in the simulation - no moving bracket was used. The frame set was then analysed by the DDT program and the number of detected lines recorded, along with the execution time to complete each analysis. A new set of frames was then generated, and the process repeated 50 times to obtain statistical analysis data. Parameters were then varied, and another 50 simulations were run.

The parameters that were varied were the number of frames (and therefore the number of dots) used to determine the existence of a straight line, and the value of sigma above mean sky level that the frames were thresholded to. The search area nominal radius was altered automatically to suit the number of frames analysed using equation 7.1, and the predicted position diameter set to a value of 3 pixels. The frames were sized to simulate a 519x519 pixel array, the same size as the real CCD images in section 8.2.

8.1.1 Noise Test Results

Graphs of DDT probability in detecting noise-induced "false alarms", plus run time for each test, are presented in Figure 8.1 and Figure 8.2.

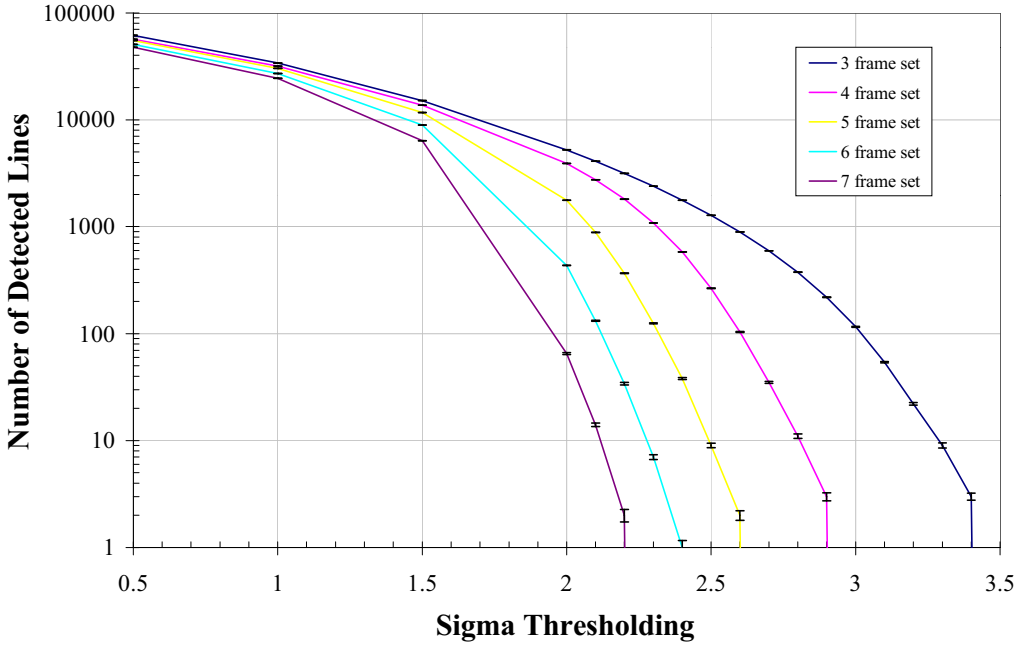

Figure 8.1: Number of spurious lines generated by noise dots for sets of frames ranging from three to seven in a set. For this simulation the predicted position diameter was three pixels.

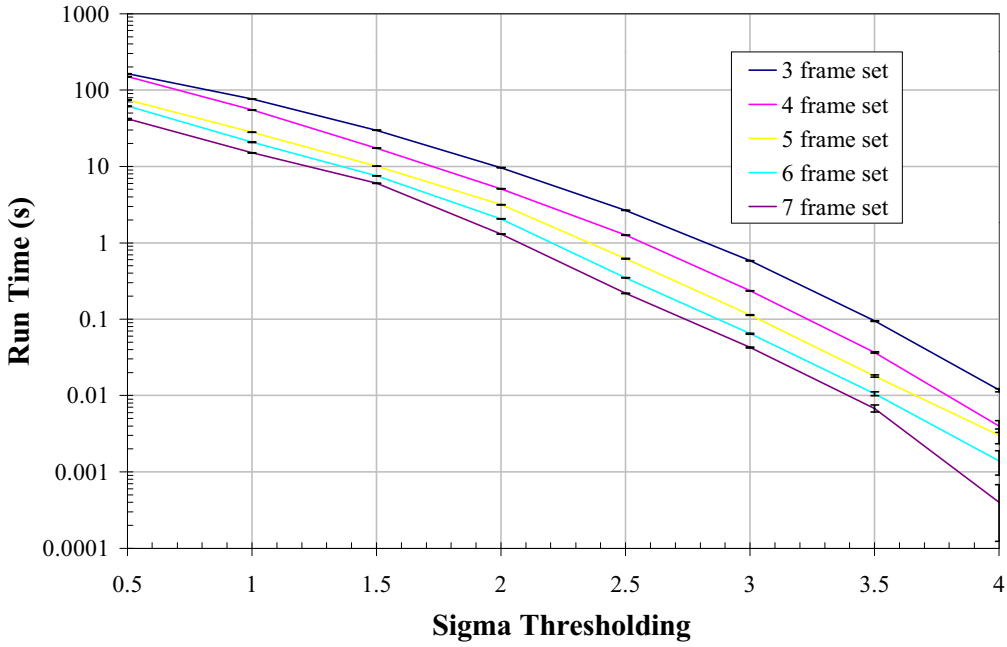

Figure 8.2: Execution time for each set of parameters. For this simulation the predicted position diameter was three pixels.

8.1.2 Static Noise Test Analysis

Figure 8.1 shows the number of detections as a function of threshold σ and it can be seen that as expected the number of noise-induced lines decreases with both the thresholding level and the number of frames per set (or dots per line). It is of interest to note however that the run time in both cases shows the three frame sets taking approximately an order of magnitude longer to analyse than the seven frame sets (Figure 8.2). This is due to the fact that the radius of the search areas in frame 2 of the analysis bracket is related to the number of frames in the bracket by equation 7.1. This means that although there are fewer frames to analyse in the case of N = 3 (N = number of frames), the search area in frame two is much larger than if N = 7. The two areas are therefore related by the quotient of the squares of (N–1), which in the case of N = 3 and 7 yields a ratio of 4/36 = 9, in close agreement with the timing results.

With reference to Figure 8.1 the minimum thresholding value to ensure no noise-induced lines is given by the intercept of each curve with the abscissa (i.e. number of detected lines < 1). As the resolution of the graph is accurate to 0.1σ, the next highest increment in σ is taken to be the thresholding value. The minimum thresholding value with respect to N, σ_{min} , is therefore given by:

N	3	4	5	6	7
σ_{min}	3.5	3.0	2.6	2.4	2.3

Table 8.1: Empirical results of the minimum thresholding value required to reduce the number of noise-induced tracks of length N to one or less.

A power-law fit to this data gives equation (8.1) which can be extrapolated to higher values of N (Figure 8.3):

$$\sigma_{min} = 6.0814\ N^{-0.5121}. \qquad (8.1)$$

Figure 8.3 can therefore be used to determine the correct minimum thresholding value for any given number of dots per frame, for a given number of pixels per image.

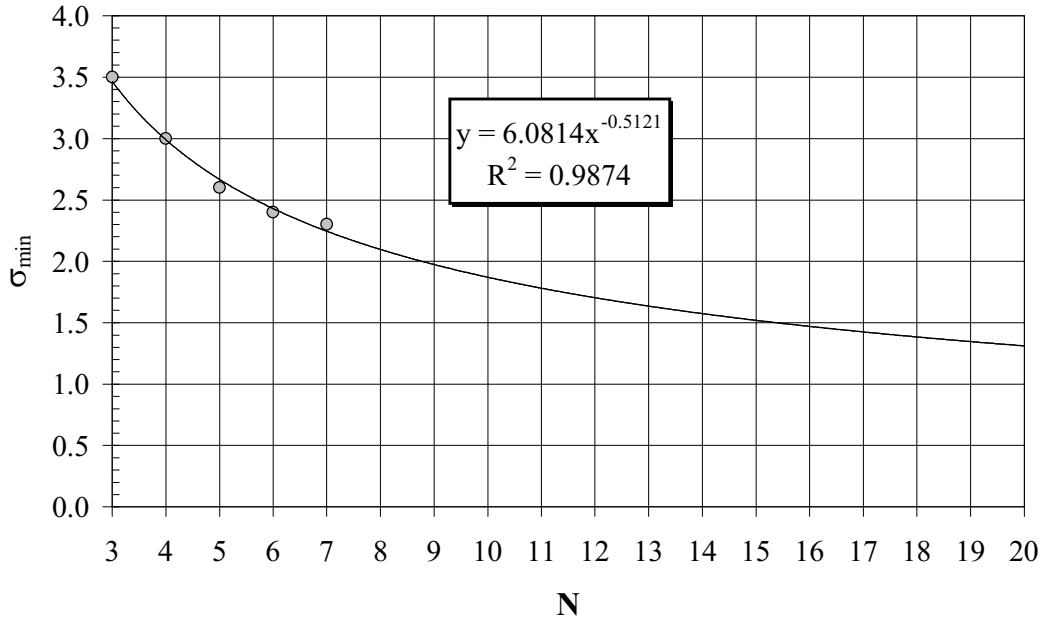

Figure 8.3: Minimum threshold value to ensure less than one noise-induced track. Given a FOV and frame interval, the number of noise dots per frame must be reduced to a level such that the chances of a noise-induced track being formed are minimised. This level corresponds with the value of σ_{min} . Empirical data are plotted in the range N = 3-7, and a power law fit is used to extrapolate to higher values of N.

8.2 South Africa Image Testing

8.2.1 Introduction

The images in this section were taken on 10th November 1996 at 02h UT at the South African Astronomical Observatory Station (SAAO) at Sutherland, South Africa. The observers were Dr Simon Green and Michael Foster. Full details of the observatory, telescope and CCD camera are given in Table 8.2.

Thirteen images were obtained with an average frame interval of 45s. All images were taken with the telescope pointed at the zenith and the drive system off. Full details of the pictures are given in Table 8.3.

Latitude	32.3794º S
Longitude	20.8107º E
Elevation	1798m
Primary diameter	1.0m
f-ratio	16
Camera	TEK8
CCD size	512×570
Plate scale	0.348” pixel^{-1}
FOV	180.612”

Table 8.2: Details of the 1m telescope and camera system at SAAO.

File Number	T_{int} (s)	UT (h:m:s)	T_{cyc} (s)
1	0.142	02:36:00	
2	0.142	02:37:03	63
3	0.141	02:37:39	36
4	0.141	02:38:15	36
5	0.142	02:39:13	58
6	0.143	02:39:56	43
7	0.142	02:40:39	43
8	0.141	02:41:31	52
9	0.141	02:42:10	39
10	0.142	02:42:57	47
11	0.142	02:43:36	39
12	0.142	02:44:13	37
13	0.142	02:45:00	47
Mean	0.141769	Mean	45

Table 8.3: Details of the picture files taken at SAAO. Column 1 is the file designation number, column 2 is the integration time for each image, column 3 the time of each integration to the nearest second, and column 4 is the interval since the previous image, expressed as the cycle time T_{cyc}.

8.2.2 Image manipulation

As the DDT program was originally designed for pictures consisting of lists of dots (centroids), the raw images from SAAO were post-processed into a form compatible with these input parameters, to simulate an image stream from the camera front end. Starlink astronomical image processing packages, namely KAPPA and FIGARO, were used for this purpose. The method followed is given below. All stages are standard image processing techniques for astronomical CCD images.

1. Correct for brightness value wraparound. The 16-bit pixel brightness values on the CCD camera at SAAO wrapped around from 0 to 32768, then -32768 to -1, with increasing brightness. To unwrap the brightness values to the more useful 0 to 65536 range, the following equation (8.2) in the MATH routine in KAPPA was used, where $b_{1,2}$ are the original and new brightness levels, respectively:

$$b_2 = b_1 + \left\{ 32768 \cdot \left[\frac{b_1}{-|b_1|} + 1 \right] \right\}. \qquad (8.2)$$

2. Subtract bias frame. If the CCD shutter is closed and a zero-second exposure read off, an image is still produced that is intrinsic to the detector. This bias frame was subtracted from all frames using the SUB function in KAPPA.
3. Renumber the X,Y coordinate axes using the LXSET & LYSET functions in FIGARO.
4. The DDT program currently can only analyse square images, so frames are cropped to conform with this format, using the ISUBSET function in FIGARO.
5. Divide through by the flatfield image using the DIV function in KAPPA.

In addition to these processes, the images were then thresholded and centroided; this was accomplished with software especially developed for the purpose by the Starlink Quick Response software solutions team. The software enabled the thresholding sigma level to be selected manually.

8.2.3 Results

Two effects conspired to render the SAAO images unsuitable as a test bed for the DDT program. The first was that the only mean frame rate possible with the CCD camera was 0.02 Hz, or 1 frame every 45 seconds (Table 8.3). Given that the FOV was 180.612", the frame interval 45s, and the minimum number of dots to form a line being 3, this implied a maximum value of ω_{top} of:

$$\omega_{top} = \frac{180.612''}{2 \times 45s} = 2.007''s^{-1}, \tag{8.3}$$

for any object to be detected, which in turn implied that the circular orbital height must be no lower than an initial estimate of ≈ 150,000km (using equation 7.6). This is a far greater height than any space debris orbit (over 4 times GSO height) and therefore any objects visible at such heights fall outside the remit of this investigation. Lower debris would pass through the FOV before at least 3 frames were taken.

The other effect was that the frames were taken at irregular intervals (Table 8.3 again); this precluded any possibility of detecting a body by its uniform motion against a noisy background, as the DDT program was configured then only to do this.

The images were still used however as raw data for a proof-of-concept trial run of the DDT program to demonstrate its ability to process the type of data the camera system at Herstmonceux would have provided it in the original concept.

The images were processed in the manner outlined above and the DDT program configured to detect an object passing through the FOV at a speed to produce a minimum of 4 dots in its track. For this value of N, the required minimum thresholding limit to minimise noise-induced tracks was 3σ, which would have given ~350 dots per frame. Unfortunately the external thresholding and centroiding program failed to perform its task to the level of accuracy required, in that the mean number of dots per frame produced was 3913. The very short integration time precluded the possibility that the presence of many stars may have caused this effect; the conclusion was reached that the thresholding/centroiding software was faulty.

The mean number of dots present in each frame however corresponds to a sigma level of approximately 2.2, which by Figure 8.3 implies a value of N of ≈ 7.4 to ensure no noise induced lines. As only integer values of N are possible however, DDT program runs were performed for N values of both 7 and 8. The resulting number of tracks detected for each run are given in Table 8.4.

N value	7	8
No. of tracks	10	0

Table 8.4: Number of detected tracks for values of N either side of the corresponding thresholding limit for noise-induced tracks.

This is in keeping with the theory that noise-induced tracks should begin to appear for track lengths of 7 dots and under; i.e. if there were any debris objects in the field of view (of a size to be visible) they would have been detected for N = 8 (had the frame rate been regular).

To test all functionality of the DDT program however, the objects detected were analysed by the software for their orbital characteristics (Table 8.5), though as previously stated, the fact that the frames were taken at irregular intervals precludes any possibility that the tracks are anything other than noise. The track data are presented in Table 8.5 and Figure 8.4.

Track Number	Topocentric angular speed (“ s^{-1})	Orbit Height ($\times 10^5$ km)	Inclination (degrees)
1	0.562	3.752	147
2	0.539	3.859	132
3	0.412	4.620	157
4	0.570	3.717	122
5	0.292	5.817	115
6	0.583	3.661	53
7	0.556	3.779	58
8	0.549	3.812	34
9	0.585	3.652	157
10	0.514	3.984	118

Table 8.5: Orbit height and inclination calculated from trajectory analysis of the ten tracks detected with the DDT. Inclinations are accurate to the nearest degree only, due to the similar accuracy of knowledge of the CCD orientation in the focal plane.

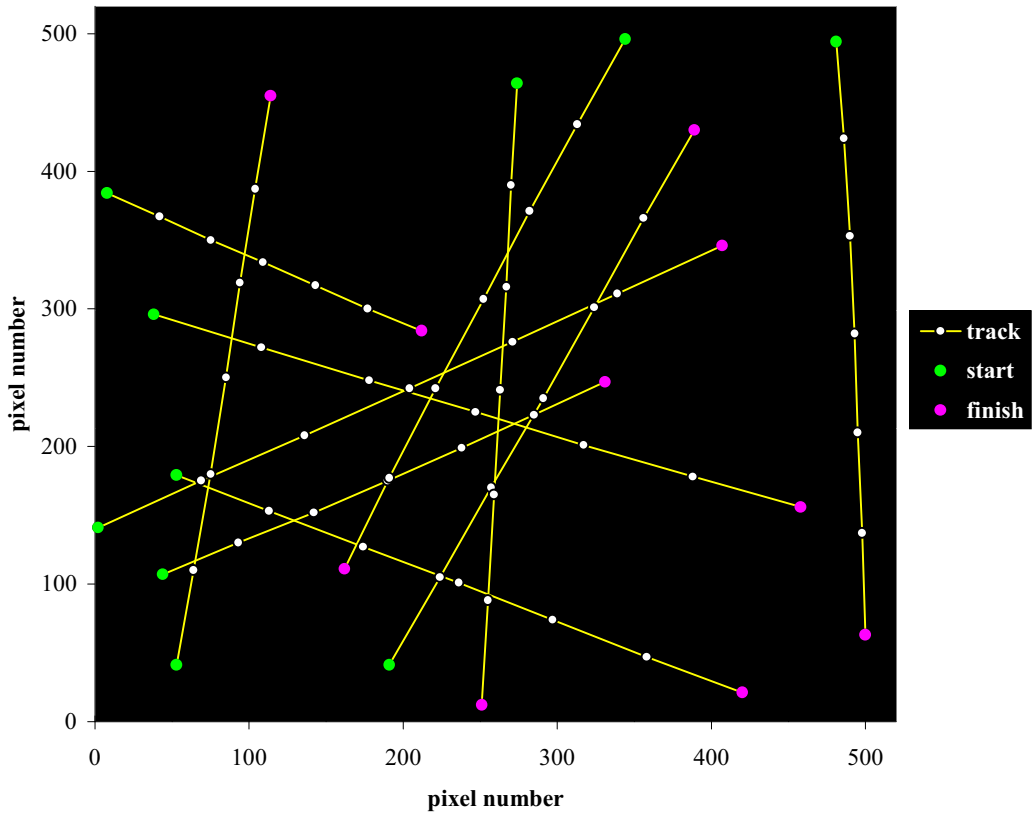

Figure 8.4: demonstration of tracks detected by the DDT program. The irregularity of the frame rate, plus the thresholding level below the minimum required to exclude noise-induced lines mean that all of these tracks are noise-induced. Tracks beginning and end are colorcoded to indicate direction.

8.3 Minimum Detectable Size of Debris

8.3.1 Minimum altitude

For a given FOV and frame interval, there is a minimum altitude that debris will be detected. The fastest and therefore lowest debris that can be accommodated by the DDT program is that which forms a line of 3 dots (such that N=3) across the FOV. This was mentioned briefly in section 7.5, and is dealt with in more detail here. Equation 7.5, reiterated here as equation (8.4), shows the relationship:

$$\omega_{top} = \frac{FOV}{2T_{cyc}} \ . \tag{8.4}$$

The orbital height is obtained for both tracking and non-tracking cases by rearranging the expressions for ω_{top} to solve for the semimajor axis a, obtaining a cubic in $a^{1/2}$.

For the sidereal tracking case:

$$a^{3/2} - r_e\, a^{1/2} - \frac{\mu^{1/2}}{\omega_{top}} = 0 \, . \tag{8.5}$$

For the non-tracking case:

$$a^{3/2} - \left[\frac{r_e\, \omega_{top}}{\omega_{top} + \omega_o}\right] a^{1/2} - \left[\frac{\mu^{1/2}}{\omega_{top} + \omega_o}\right] = 0 \, . \tag{8.6}$$

Both cubics are of the form $\mathbf{x^3 - Ax - B = 0}$, the solution to which is given by (de Heer, 1999):

$$x = \frac{Z^{\frac{1}{3}}}{6} + \frac{2A}{Z^{\frac{1}{3}}} \ , \tag{8.7}$$

where

$$Z = 108\, B + 12\sqrt{\left(-12\, A^3 + 81\, B^2\right)} \ . \tag{8.8}$$

NB: The square root term is negative for many values of A and B, making Z a complex number in that case.

If T_{cyc} could be varied infinitely, i.e. made as small as one wished with no restrictions due to instrumenation speed limits, the results of varying T_{cyc} would look like Figure 8.5, where curves of h vs T_{cyc} for both tracking and non-tracking cases are shown.

The maximum possible time for a value of T_{cyc} corresponds to the length of the night. A maximised amount would be at the equator during equinox, with a value of the order of 9.6 hours (marked on the graph), which is the time between astronomical dusk and dawn. The asymptote at ≈ 36000km is geostationary orbit (GSO), for which T_{cyc} tends to infinity.

In practice however, the finite analysis time of the images imposes a restriction to how low T_{cyc} can go. This is discussed and illustrated in the next section, using worked examples of analysis time for select cases.

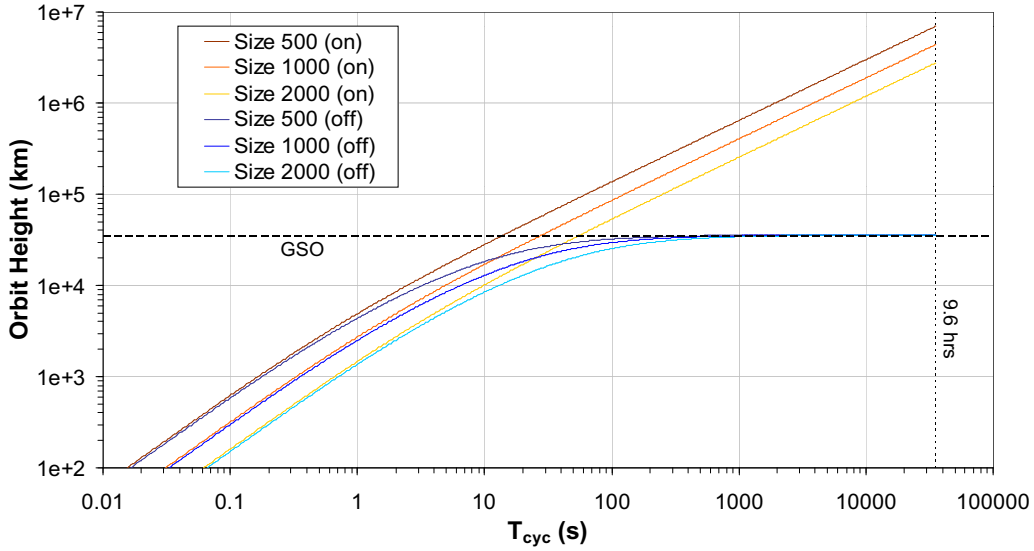

Figure 8.5: Plot of orbit height as a function of the cycle time T_{cyc} for cases where sidereal tracking of the telescope is both on and off. In each tracking situation the height is calculated for three sizes of CCD (519, 1000 and 2000 pixels on a side). See text for more details.

8.3.2 Minimum Debris Size

For any height calculated in the previous section, a minimum size of debris capable of being detected by the DDT can be calculated. Only the simple case of a 2D coplanar system (equatorial circular orbit, equatorial site, zenith viewing) is discussed here.

The cycle time is made up of three parts, the integration time T_{int}, the readout time T_{read}, and the analysis time T_{an}, so that:

$$T_{cyc} = T_{int} + T_{read} + T_{an} \, . \qquad (8.9)$$

The integration time is assumed to be matched to the dwell time, the time taken for the debris image in the focal plane cross one pixel, which is assumed to be matched to 1 arcsecond:

$$T_{dwell} = \frac{(\text{pixel size})}{\omega_{top}} \quad . \tag{8.10}$$

Values of dwell time with orbital height are shown in Figure 8.6.

The analysis time is a function of the size of CCD (in pixels), the thresholding value adopted (in sigma), and of course the speed of the computer. In section 8.1.2 the minimum amount of thresholding required to prevent false alarms (noise-induced lines) for a 519×519 pixel CCD at N=3 was found to be σ_{min} = 3.5, and the analysis time T_{an} was 0.1s. In this section CCD sizes of 1000 and 2000 pixels square will be considered, so σ_{min} and T_{an} was calculated in the same manner for these size arrays, and the results tabulated below (Table 8.6).

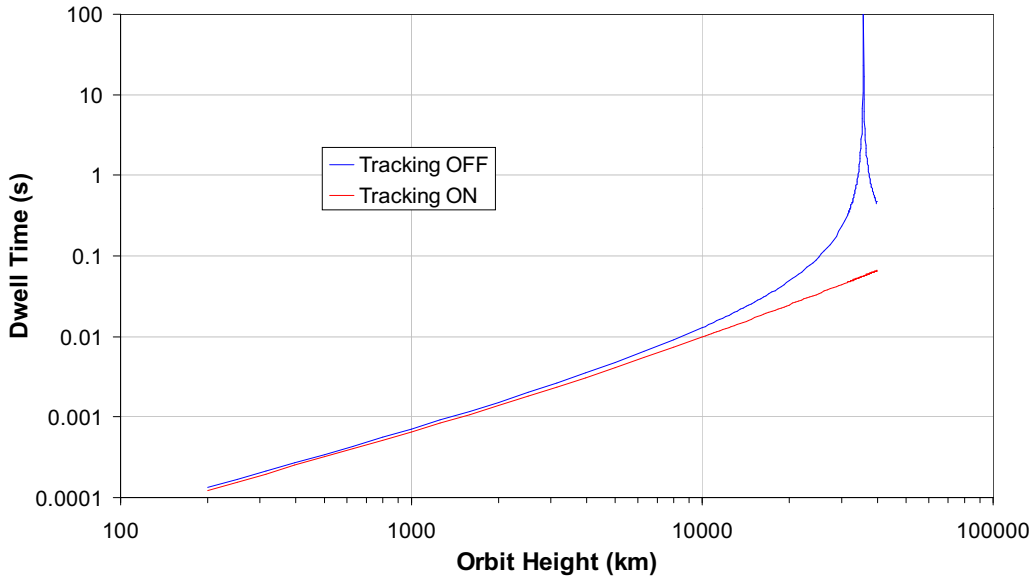

Figure 8.6: Dwell time as a function of orbit height for a zenith-looking telescope at an equatorial site, and an equatorial circular orbit. The pixel is taken to be 1 arcsecond in size, and curves for situations when sidereal tracking is both off and on are shown.

CCD size (pixels square)	σ_{min} (for N=3)	T_{an} (s)
519	3.5	0.10
1000	3.8	0.30
2000	4.0	1.99

Table 8.6: Minimum thresholding to ensure no noise-induced false lines, plus the analysis time to perform the analysis, using a 350MHz Pentium PC running Linux RedHat 5.2.

Given values of T_{int} and T_{an}, and knowing T_{cyc}, equation (8.9) gives a value for T_{read}. This is the amount of time it takes to read the CCD image. The transfer rate is given by:

$$R_{read} = \frac{N_{pix}}{T_{read}} \text{ (pixels sec}^{-1}\text{)}. \qquad (8.11)$$

which directly influences the readout noise. From typical values of readout noise with readout rate for CCDs at the Isaac Newton Group (ING) of telescopes at La Palma (Carter, 1994) and at the Anglo-Australian Observatory (AAO) in Australia (Ryan and Fish, 1995), one can derive that a power law relationship best fits the data (Figure 8.7). In recent years however, the new FIERA (Fast Imager Electronic Readout Assembly) CCD readout & amplifier controller at the European Southern Observatory (ESO) is delivering very low readout noise for high readout rates (Cumani and Donaldson, 1997). It is hoped in the future that readout noise will be in the subelectron level for readout rates of 50 megapixels s^{-1}, but for now typical rates are quoted as $2e^-$ for 100 kilopixels s^{-1}, rising to about $5e^-$ for 1 megapixel s^{-1}. Assuming a power law fit to these values as well, an expression for the readout noise signal S_r as a function of readout rate using the FIERA controller can be derived as:

$$S_r = 0.0205\, R_{read}^{\,0.3979} \ (e^-)\,, \qquad (8.12)$$

with R_{read} being the rate in pixels sec^{-1} (Figure 8.7).

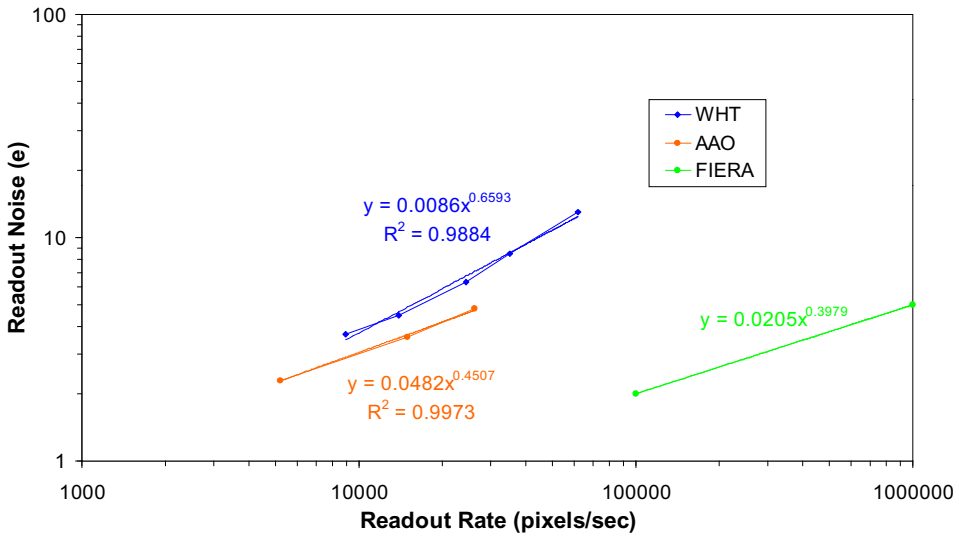

Figure 8.7: Readout noise rates for CCDs at the William Herschel Telescope (WHT) and Anglo-Australian Telescope (AAO), plus rates for the FIERA CCD controller. Power law fits are also shown for the data.

A moonless night was assumed, with sky background flux levels due to airglow (F_{sky}), galactic background (F_{gal}) and zodiacal light (F_{zod}) reduced to the following values: $F_{sky} = 5.98\times10^{-20}$ W m^{-2} nm^{-1} arcsec^{-2}; $F_{gal} = 50\ S_{10} = 1.325\times10^{-20}$ W m^{-2} nm^{-1} arcsec^{-2}; $F_{zod} = 150\ S_{10} = 3.975\times10^{-20}$ W m^{-2} nm^{-1} arcsec^{-2}. The total flux was therefore taken to be a constant F_k being the sum of these fluxes, so that $F_k = 1.128\times10^{-19}$ W m^{-2} nm^{-1} arcsec^{-2}.

The power P_k of this flux at the telescope objective is

$$P_k = \frac{F_k\ A_{tel}\ Ext\ \Delta\lambda\ \rho}{E_{phot}}\ \ (W)\ , \tag{8.13}$$

where A_{tel} = objective area (m^2), Ext = extinction factor = 0.9 (assuming zenith viewing at a good site), $\Delta\lambda$ = 300nm, ρ = efficiency of the system (optics transmission and DQE of CCD) = 0.53, E_{phot} = energy of one photon = 3.6118×10^{-19} J. All of these values are taken from the typical values used in Chapter 4.

The signal S_k in electrons is therefore given by:

$$S_k = P_k\ \tau\ platescale\ , \tag{8.14}$$

where τ is the integration time (s) matched to dwell time, and platescale is matched to 1 arcsecond per pixel.

Putting all of the above values into equations (8.13) and (8.14) gives:

$$S_k = 44.69\ A_{tel}\ \tau\ \ (e^-)\ . \tag{8.15}$$

Rearranging the SNR equation defined in Chapter 4, we get a quadratic in S_d, the debris signal, as a function of the SNR (chosen to be 3, as in chapter 4), and the readout and sky background signals calculated above:

$$S_d = \frac{\left(2\,S_r\,SNR + SNR^2\right) + \left[\left(-2\,S_r\,SNR - SNR^2\right)^2 - 4\left(SNR^2 S_r^2 - SNR^2 S_k\right)\right]^{\frac{1}{2}}}{2}\ . \tag{8.16}$$

Given that:

$$S_d = \frac{P_{tel}\ \tau\ \rho}{E_{phot}\ A_{streak}}\ (e^-\ pixel^{-1})\ , \tag{8.17}$$

we get:

$$P_{tel} = \frac{S_d\ E_{phot}\ A_{streak}}{\tau\ \rho}\ . \tag{8.18}$$

Also, from chapter 4,

$$P_{tel} = I_{deb}\,\Omega_{tel}\,\mathrm{Ext}\,\Delta\lambda\,, \tag{8.19}$$

where Ω_{tel} = solid angle of telescope objective, Ext and $\Delta\lambda$ are as defined above, and I_{deb} is given by:

$$I_{deb} = \frac{\mathrm{Sol}_{600}\,\pi r_{deb}^2\,A_b(\phi)}{\pi}\ (\mathrm{W\ nm^{-1}\ sr^{-1}}), \tag{8.20}$$

where sol_{600} = solar flux per nanometre at 600nm = 1.752 W m^{-2} nm^{-1}, and $A_b(\phi)$ is the Bond albedo. For this instance we take the phase angle to be zero, so that $A_b(0) = 0.22$.

Solving (8.20) for r_{deb}, converting to a diameter d_{deb}, and substituting (8.19) in for I_{deb} gives:

$$d_{deb} = 2\left[\frac{P_{tel}}{\Omega_{tel}\,\mathrm{Ext}\,\Delta\lambda\,\mathrm{sol}_{600}\,A_b(0)}\right]^{\frac{1}{2}}\ (\mathrm{m}). \tag{8.21}$$

Use of equations (8.9) to (8.21) lead therefore to the derivation of d_{deb} as a function of orbital height. Results for tracking and non-tracking systems with CCD sizes of 519, 1000 and 2000 pixels square (corresponding to fields of view of 0.14°, 0.28° and 0.56° respectively) are shown in Figure 8.8 and Figure 8.9 respectively, for an amateur 8-inch (20.3cm) Schmidt-Cassegrain telescope (SCT), and 1m and 2m telescopes.

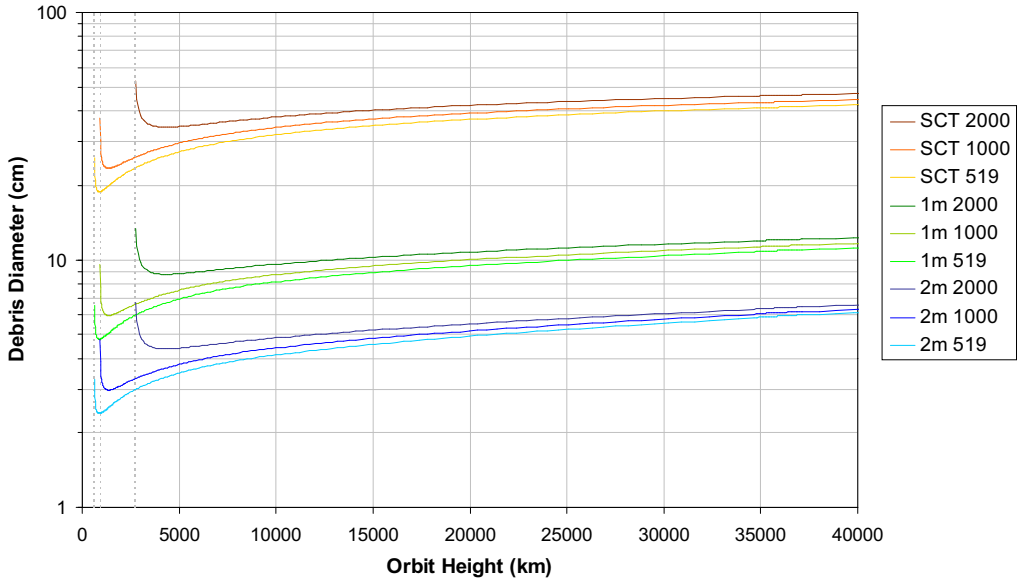

Figure 8.8: Graph of minimum detectable debris diameter for 519, 1000 and 2000 pixel square CCDs for a 10-inch SCT (orange grouping), and 1m & 2m telescopes (green and blue groupings respectively). Legend indicates telescope type and CCD size respectively for each curve. Vertical dashed lines indicate cutoffs due to finite minimum cycle time. See text below for details.

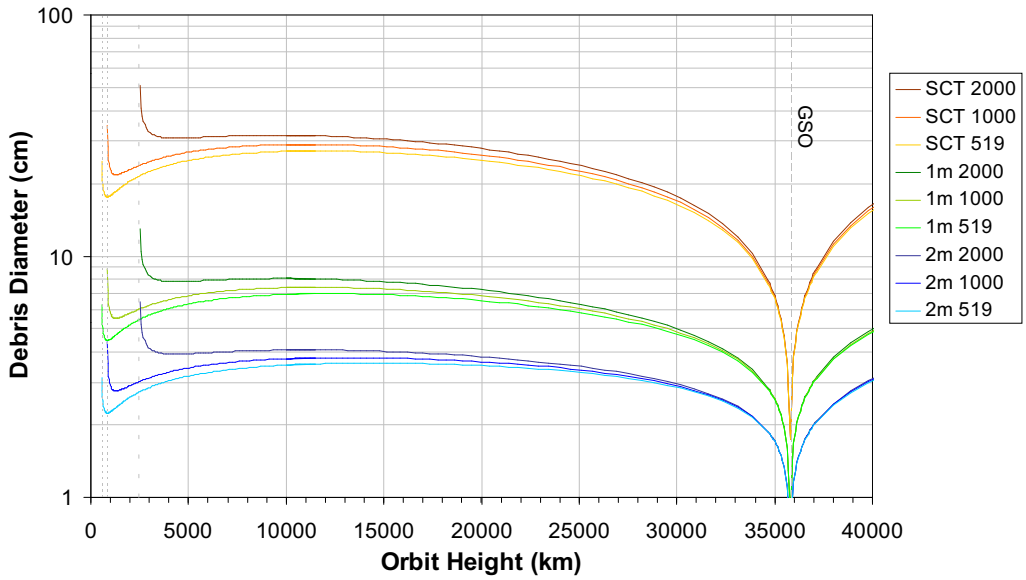

Figure 8.9: As for Figure 8.8 but for the non-tracking case. Additional dashed line at ≈36,000km denotes geostationary orbit height.

A low-altitude cutoff exists for debris detection, due to the finite analysis time of the images. Recalling from equation (8.9) that $T_{cyc} = T_{int} + T_{read} + T_{an}$, each size of CCD has a corresponding minimum analysis time T_{an} to ensure no false alarms (Table 8.6). T_{int} is fixed also to the dwell time to ensure full pixel coverage of the debris image. Therefore as T_{cyc} reduces with orbit height, T_{read} must reduce also. The limiting case of detectability therefore is when T_{read} is zero. As T_{read} approaches zero (as orbit height decreases), the readout rate tends to infinity, causing the debris size necessary to cause a SNR of 3, to rise to infinity also.

This limiting case threshold may be calculated by setting T_{read} to zero in equation (8.9) and equating T_{cyc} with equation (8.4) to obtain:

$$T_{int} + T_{an} = \frac{FOV}{2\,\omega_{top}} \,. \tag{8.22}$$

But the integration time is matched to the dwell time, which is defined in equation (8.10). Substituting this into (8.22) and equating for ω_{top} gives:

$$\omega_{top} = \frac{\left(\frac{FOV}{2} - pixelsize\right)}{T_{an}} \,. \tag{8.23}$$

Calculating orbit height from ω_{top} for the three cases of FOV of the 519, 1000 and 2000 pixel square CCDs, for which T_{an} is already known, gives the following selected cases (Table 8.7).

FOV (arcsec)	T_{an} (s)	ω_{top} (arcsec s^{-1})	Orbit Height (km)	
			Tracking ON	Tracking OFF
519	0.10	2585.00	603	564
1000	0.30	1689.23	903	843
2000	1.99	502.01	2720	2489

Table 8.7: Orbit height corresponding to minimum detectable debris, due to timing constraints only. See text for details.

These values therefore effectively represent the orbit height limits below which the debris is travelling too fast for the DDT system as a whole to keep up. These heights are marked on the graph as vertical dashed lines, and asymptotic behaviour can be seen for the debris size curves as height decreases to these limits. Sampling frequency of the generating code results in finite cutoff of the curves near the asymptotes.

The rest of the general shape for all of the curves as one increases orbit height can be explained with reference to the example curve for a 1000×1000 pixel CCD and a 10-inch SCT for both tracking and non-tracking cases (Figure 8.10).

A. Cutoff due to timing constraints as described above.
B. Downslope because the debris' ω_{top} is slows with height, causing lower readout noise & thus increasing S_d & causing d_{deb} to fall.
C. Although ω_{top} reduces as one increases orbit height, the debris is further away and thus is getting fainter with distance, so that d_{deb} rises to maintain a SNR of 3.

(*the following apply to non-tracking case only*)

D. ω_{top} decrease (as height approaches GSO) overrides the effect due to increased distance, i.e. dwell time is longer.
E. Dip at GSO – debris is effectively stationary.
F. Debris exhibits retrograde motion above GSO and magnitude of ω_{top} increases.

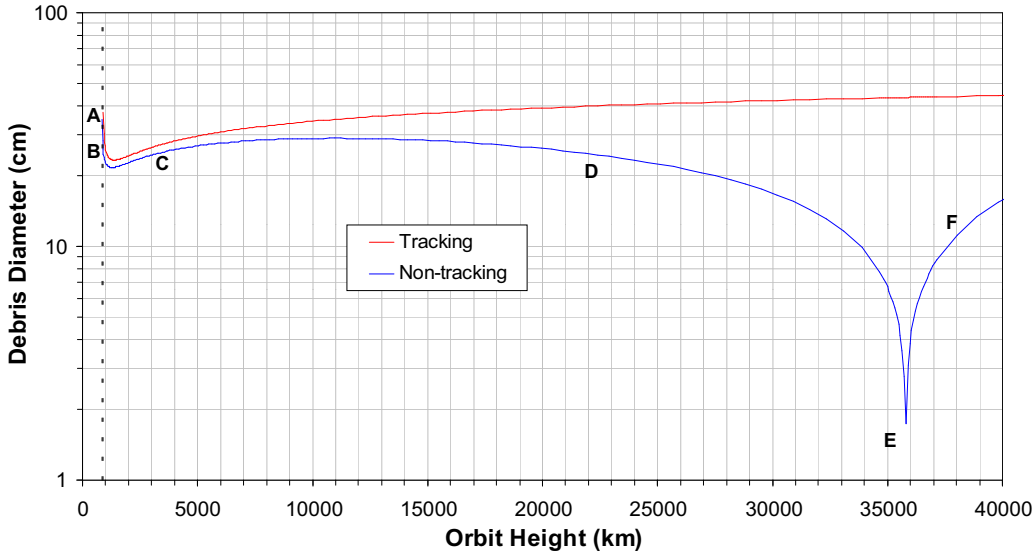

Figure 8.10: Comparison between tracking and non-tracking of telescope to sidereal rate for chosen example of 10-inch SCT with 1000×1000 pixel CCD array, corresponding to a FOV of 1000 arcsec. Letters describe curve characteristics in the main text.

It can be seen that although for larger CCDs the debris size detectability is slightly worse (because of the increased analysis time), the difference between size obtained with a 519×519 pixel CCD and one with 2000×2000 pixels is of the order of 1cm or less for 1m telescopes or larger, for heights above ~10,000km. The extra spatial and angular resolution afforded by the larger CCD would enable more refined orbit calculations, as well as covering a larger volume of space.

Another effect of increasing CCD size (and therefore FOV) is the slower process time (readout + analysis) that causes the cutoff at point A on Figure 8.10. The larger FOV does not help by increasing the time spent in the FOV by debris in this case. A 2000×2000 pixel CCD compared to a 519×519 affords an increase in possible analysis time of a factor of ~4, but the actual analysis time increase is more like a factor of 20 (Table 8.6).

8.4 Conclusions

With respect to the static tests of performance, Figure 8.1 shows that the DDT program appears to be more suited to the detection of slower debris. For a given number of noise dots per frame, it takes more time for the program to detect any

lines from a set of three frames than it does from larger sets. For distant debris objects this is not a problem, since those in higher orbits have a slower topocentric angular speed and the increased time it takes to cross the FOV would offset the longer process time. However for debris in lower and therefore faster orbits, the longer process time causes a cut-off in the minimum height for a particle that could be detected by the program.

With a wider FOV and a higher frame rate, the DDT program could function adequately and detect a regularly-moving object that appeared above the SNR for its appropriate dwell time. All aspects of the program performed as they should, despite the quality of the raw images analysed.

Under similar conditions, the size of debris that can just be detected with a SNR of 3 for a given height is slightly smaller for a non-tracking telescope than for a tracking telescope. This is due to the slower topocentric angular speed caused by the vector subtraction of the Earth's sidereal rate from the geocentric angular velocity of the debris. In LEO this difference is small as the geocentric angular velocity of the debris is an order of magnitude greater than the Earth's sidereal rate, but close to GSO the difference becomes larger. This effect is evident in Figure 8.10.

Typical debris sizes detectable under these conditions are below ~10cm for 1–2m class telescopes for all heights, and below ~50cm for a typical amateur 10-inch SCT (Figure 8.8 & Figure 8.9).